Chemie der Erde 77 (2017) 267–279

Contents lists available at ScienceDirect

Chemie der Erde

journal homepage: www.elsevier.de/chemer

Mopping up leaking carbon: A natural analog at Wadi Namaleh, Jordan

Nizar Abu-Jaber

Department of Civil and Environmental Engineering, German Jordanian University, Amman, Jordan

ARTICLE INFO

Article history:
Received 29 October 2016
Received in revised form 24 February 2017
Accepted 3 April 2017
Editorial handling - Alexander Deutsch

Keywords:
Surface alteration
CO_2
Carbon capture and sequestration
Greenhouse gas emissions
Jordan
Surface processes

ABSTRACT

Carbon capture and sequestration (CCS) is one of the important options available for partially stemming greenhouse gas emissions from large point sources. The possibility of leaking from deep storage needs to be addressed. The Wadi Namaleh area in southern Jordan provides an interesting case study of how excess CO_2 can be trapped in the form of carbonates in the near surface, even when the local geology is not obviously conducive for such a process.

Carbonate veins are formed in surface alteration zones of rhyolite host rock in this arid region. The alteration zones are limited to areas where surface soil or colluvium are present. Oxygen, deuterium and carbon isotopes of the carbonates and near-surface ground water in the area suggest that the source of carbon is deep seated CO_2, and that the carbonate precipitated in local meteoric water under ambient temperature conditions. Analysis of strontium in the carbonate, fresh rhyolite and altered host shows that the source for calcium is aeolian. Trace elements show that metal and REE mobility are constrained to the alteration zone.

Thus, interaction of H_2O, CO_2 and atmospheric wet and dry deposition lead to the formation of the clayey (montmorillonite) alteration zone. This zone acts to trap seeping CO_2 and water, and thus produces conditions of progressively more efficient trapping of carbon dioxide by means of a positive feedback mechanism. Replication of these conditions in other areas will minimize CO_2 leakage from man-made CCS sites.

1. Introduction

Growing concern over rising atmospheric CO_2 levels and the climatic implications for that have led to various proposals to dampen this trend. One set of proposals calls for sequestration of CO_2 from large point sources into deep saline aquifers (Benson and Cole, 2008). This process is in use in a number of locations around the world, and is generally known as carbon capture and sequestration (CCS). The gas is cooled and pressurized to convert it into liquid form, and injected into sealed aquifers or depleted hydrocarbon reservoirs. Under subsurface conditions, four types of CO_2 trapping occur, which are structural (CO_2 in a liquid form floating over the groundwater and below a cap rock), capillary (liquid CO_2 trapped in pore spaces with water), solubility (CO_2 dissolved in water) and mineral tapping (carbon trapped in solid carbonate mineral form; Benson and Cole, 2008). Over the short-term, it is envisioned that structural trapping is the most significant, with the solubility and mineral trapping progressively gaining significance through time (Benson and Cole, 2008). Clearly, the solid form is the most desirable for perpetual storage.

Numerous technical and environmental issues arise from CCS. For example, it has been reported that pressure changes induced by CO_2 storage has triggered seismicity at some CCS sites (Häring et al., 2008). Moreover, the pressure fronts may extend far beyond the injection zones to create near-surface deformation (Rutqvist, 2012). This may induce the possibility of more leaking with time. Injection induced stress may cause the formation of micro-cracks, which may inadvertently lead to leakage out of the storage area (Rutqvist, 2012). This, in turn, may lead to geochemical processes that may contaminate the overlying aquifers.

Little and Jackson (2010) conducted a series of laboratory experiments to discern the effect of leaking CO_2 on the hydrochemistry of a group of aquifer waters and materials (most of which were loose sands). These were designed to deduce the effect of CO_2 leakage on groundwater residing in aquifers that overlie CCS storage spots. These experiments showed that a CO_2 flux through these aquifers would generally lead to significant increases in the concentrations of alkalis, alkali earths, nickel, barium and iron in the groundwater. These changes in chemistry occurred within 2 weeks of the initiation of the 300 day experiment, with little change thereafter (Little

E-mail address: nizar.abujaber@gju.edu.jo

http://dx.doi.org/10.1016/j.chemer.2017.04.001

and Jackson, 2010). Ueda et al. (2005) had conducted experiments under elevated temperature and CO_2 saturated water under high pCO_2 conditions in labrodorite and in granodiorite rocks. They arrived at similar results, whereby CO_2 charged water has the ability to extract calcium and silica at significantly higher levels than from distilled water. Similarly, Lo Ré et al. (2014) conducted experiments on granite and epidote samples, and yielded similar reaction products of illite and smectite clay minerals. Holzheid (2016) has reviewed much of the data regarding CO_2-water-mineral interactions, and concludes that kinetics are largely driven by brine salinity and temperature rather than pCO_2. Rempel et al. (2011) demonstrated that dissolution of metals is only appreciable in the presence of water, with very low metal solubility in pure dry pressurized CO_2.

Studies of a natural analog site where deep sourced CO_2 is leaking into shallow aquifers in New Mexico by Keating et al. (2010) suggest that solute mobilization at depth may have detrimental effects on some wells. The evidence from their study area suggest that near-surface geochemical reactions have little effect on the groundwater chemistry. This work has concentrated on the water of the aquifers, and not the resulting changes in rock material, which may provide more insight into the movement and fate of some heavy metal contaminants over longer terms.

The experimental nature of most of these studies precludes the assessment of the long-term effect of CO_2 rock interaction and the nature of the mineral trapping that may result. Also, the fate of leaking CO_2 may not be simply release into the atmosphere, but may partially result in near-surface trapping in mineral form. Thus, while carbonate is inferred to ultimately precipitate in all of these experiments, it has not actually been demonstrated to actually do so. Thus, where, if and how carbonate may precipitate is an open question. Natural analogs of such systems are limited, and tend to be constrained to mafic and ultramafic rock matrices. For example, Abu-Jaber and Kimberley (1992a) have shown that ultramafic-hosted magnesite deposits can be attributed to upward moving CO_2-rich, water poor fluids interacting with shallow water and the host rock. Such systems have been considered to be analogs for CCS sites (Boschi et al., 2009). Experimental replication of CO_2 interaction with fine-grained ultramafic rock material has shown positive results (Pronost et al., 2011). Similar carbonate deposits have also been reported in alteration products of basalt in northeastern Jordan (Kimberley and Abu-Jaber, 2005). Because ultramafic and mafic igneous rocks are rich in alkali earths (magnesium and calcium, respectively), it is quite easy to visualize remobilization of these under acidic conditions and precipitation in the form of carbonates when pCO_2 drops and pH rises, either within the mafic/ultramafic rock body or beyond the source of the alkali-earth elements near the surface. Most of the experiments that have been conducted to assess the results of carbon-bearing fluids on aquifer materials have contained obvious Ca-bearing minerals as major components. More difficult issues may arise when the wall rocks are poor in alkali earths.

Thus, the fate of CO_2 moving through Ca-poor (or Mg-poor) rocks near the surface is more difficult to predict, and is implicitly assumed that the gas will not react with the rock and water. In this study, a natural analog of CO_2 moving through rhyolite (quartz feldspar porphyry) and depositing surficial stock work veins and crusts of calcite is described and documented. The nature of the host rock alterations and the deposited carbonates gives important insights into how leaking CCS systems will behave and how at least some of the released CO_2 will ultimately be trapped in carbonate minerals despite of that, if correct conditions are achieved. Moreover, trace element dynamics in these conditions might be better understood here. This will allow for a better understanding of how to increase CCS system efficiency and improve local environmental protection as well.

1.1. Deep CO_2 in Jordan

CO_2 rising, along with other inorganic and organic gases, has been directly observed and measured by a number of researchers, both near the rift valley as well farther to the east within the plateau region of Jordan. In addition, evidence for deep CO_2 gas rising can be inferred from a number of indirect observations.

El-Naser (1991) observed that CO_2 gas rises from springs emanating from the waters of the Kurnub Sandstone formation of the Deep Aquifer complex in northern Jordan. The source of this gas remained uninvestigated until Eraifej (2006) conducted a survey of the deep water wells along the Dead Sea rift. While the amounts of gas in the water were not measured, he showed that the gases were in disequilibrium with the dissolved bicarbonate in the water, leading to the conclusion that there is an extraneous source for CO_2. This source was attributed to oxidation of organic material within the aquifer. However, Eraifej (2006) also noted that $^3He/^4He$ ratios from the wells point to a mantle source of helium. Given that there is obvious exhalation of deep gas, the idea that the source of at least some of the CO_2 is deeper cannot be excluded. This was the conclusion drawn later by Inguaggiato et al. (2016), who likewise studied the gas content of springs along the Dead Sea rift and found elevated CO_2 and helium with distinct mantle signatures.

Kaudse (2014) studied the noble gas isotopic signatures in both the Dead Sea rift region as well as in the Azraq Oasis area in the eastern plateau. He arrived at similar conclusions whereby there is a clear mantle source of gas in both the Azraq Oasis as well as many of the wells east and west of the Dead Sea rift.

Avrahamov et al. (2015) investigated methane and other hydrocarbons emanating along the entire rift valley. The source of the hydrocarbons in the northern valley seem to be mostly the result of shallow methanogenesis, whereas in the area around the Dead Sea the methane is determined to be thermogenic, with speculation that heating of asphalt at depth is the ultimate source. Sokol et al. (2014) described calcite veins associated with bitumen, calcite veins with no bitumen signs and calcrete on the western side of the Dead Sea. Bitumen seepages are common around the Dead Sea, and are believed to originate from heating of organic-rich Upper Cretaceous source rocks (Rullkötter et al., 1985). The results of Sokol et al. (2014) suggest that there is a genetic link between the calcite, bitumen and the Maastrichtian source rocks (known in Jordan as the Muwaqqar Chalk Marl Unit) for the veins.

Atallah et al. (2001) demonstrated that faults in the Dead Sea rift area lead to the preferential movement of deep-sourced radon. Because the potential sources of radon are hundreds of meters deep due to down faulting, it is remarkable that the short-lived radon can move to the surface quickly enough to be detected there. Thus, there are multiple gases from various sources moving rapidly up through fault systems in Jordan, specifically near the Dead Sea rift.

The effect of CO_2 interaction on the water chemistry is most evident in the waters of the Deep Aquifer complex that underlies much of the eastern plateau. In a study of the hydrochemistry of these waters using an inverse geochemical modeling approach, it has been demonstrated that it is impossible to explain the chemical changes seen in the waters without a source of carbon (Abu-Jaber and El-Naser, 2016). Since these waters are fossil waters that fill Palaeozoic confined sandstone aquifers at depths reaching hundreds of meters, it is difficult to envision a source of CO_2 except what might be rising from deeper sources, as seen in the previously mentioned studies of the Azraq Basin (Kausde, 2014) and the Dead Sea Rift (Eraifej, 2006).

Evidence of deep CO_2 seepage has been noted in the past in the northeastern basalt plateau in Jordan. At Biyar al Ghussein, extensive vein carbonate precipitated in highly altered basalt has been explained by a mechanism of interaction between shallow

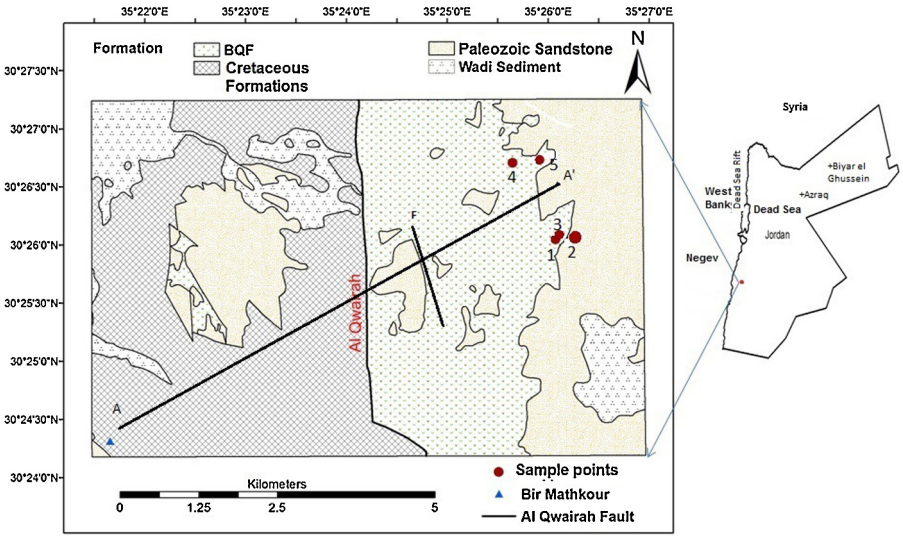

Fig. 1. Generalized geologic map of the study area (Modified after Barjous, 2003).

groundwater, deep sourced carbon dioxide and the local rocks (Kimberley and Abu-Jaber, 2005).

1.2. Study area

The study area lies about 11 km north of the ancient archeological site of Petra (Fig. 1). It lies on the eastern margin of Wadi Araba, which is part of the major Dead Sea transform fault system. In the region, block faults consisting of sets of horst and grabens showing the uplift of the Precambrian basement rock and the overlying Cambrian-Ordovician fluvial sandstones to the east of the Quwayra fault, and concurrent down-faulting to the west, exposing only Paleozoic and Mesozoic sandstones and limestones in that direction (Fig. 2).

The igneous Precambrian basement rock of Jordan (the Aqaba and Araba complexes) is widely exposed along the faults that define the contact between the rift valley in the west and the highlands of the east of the area. This basement consists of granitic and dioritic plutonic rocks, rhyolitic and andesitic volcanic rocks as well as pyroclastic deposits (Barjous, 2003). In the study area, the dominant rock belongs to the Araba complex, and more specifically the Ahaymir Volcanic Suite (Powell et al., 2015). There are four units within this suite: the Qusayb Rhyolite, the Musaymir Effusive, the Mufarqida Conglomerate and Al Bayda Quartz Feldspar Porphyry (BQP). The BQP consists of over 80% of the exposed Ahaymir Volcanic Suite and consists of reddish-pinkish rocks with visible quartz and k-feldspar phenocrysts in a fine-grained matrix (Barjous, 2003). The age of the Araba complex has been determined to be around 540–550 MA (Ibrahim and McCourt, 1995).

Overlying the Ahaymir Volcanic Suite is the Cambrian Salib Arkosic Sandstone. This formation is partially exposed in the study area, and consists of reddish-brownish sandstone. This arkose seems to be derived from the older Aqaba and Araba complex rocks, with fragments clearly visible derived from them (both granitic and rhyolitic). Subsequent Early Paleozoic formations (Abu Khushayba, Umm Ishrin and Disi Sandstones) are several kilometers away and are exposed to the east and south of the study area. These become progressively more arenitic toward the top of the sequence (Barjous, 2003).

The area in question is characterized by rugged topography imposed by hard rocks, active tectonics and arid climate. The average annual rainfall in Wadi Musa (Petra) is about 180 mm/a (Jordan Meteorological Department, 2015).

Tectonic activity in the area is related to movement along the Dead Sea transform fault system. More specifically, the Quwayra fault, with a vertical displacement of about 2.2 km and a left lateral displacement of 40 km being the dominant structural unit in the area (Barjous and Mikbel, 1990 and Barjous, 2003). The fault strikes at about 5°N, and its movement is reflected by brittle deformation in the form of faulting and jointing within the Precambrian and Palaeozoic rocks of the area. Mesozoic and Cenozoic rocks exposed to the west of the fault show more evidence of plastic deformation in the form of folds (Barjous, 2003). While the Dead Sea transform fault system has been determined to have begun in the Oligocene to Early Miocene (Barjous and Mikbel, 1990), the structural patterns in the area imprint over older patterns that date into the Palaeozoic (Barjous, 2003).

The Wadi Namaleh road connects the uplands of the Sharah mountains with the floor of Wadi Araba. The road enters the valley at the top with an elevation of 1000 m asl and the terminus of the road at the Quwayra fault is at 417 m asl; a direct line across the terrain shows a distance of about 3.7 km (thus a slope of about 16%). At the rim of the escarpment, sandstones from the Abu Khushayba and Umm Ishrin formations are exposed. Along and beginning at

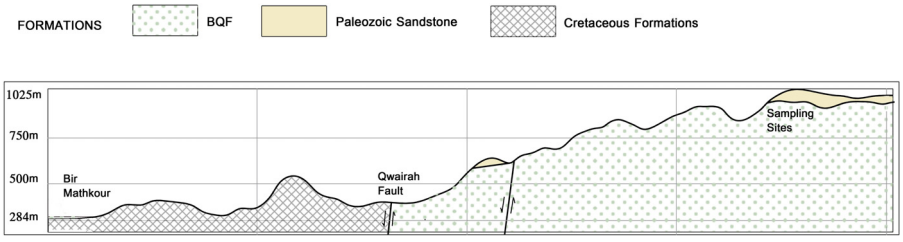

Fig. 2. Simplified geological cross section through the study area.

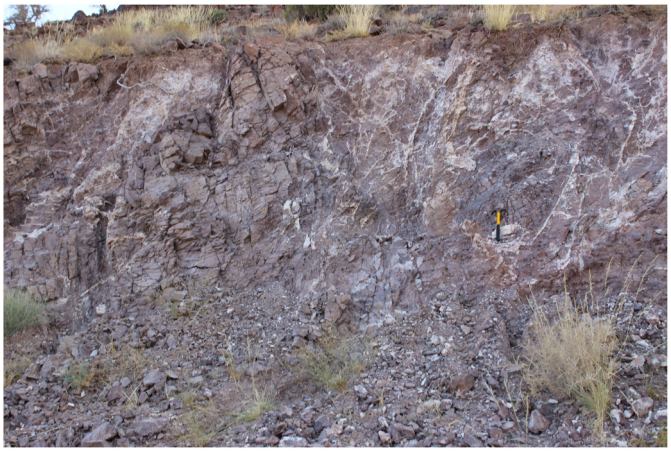

Fig. 3. General view of WN 1. Note the unaltered zone in the center of the frame in comparison to the altered zones on the left and right.

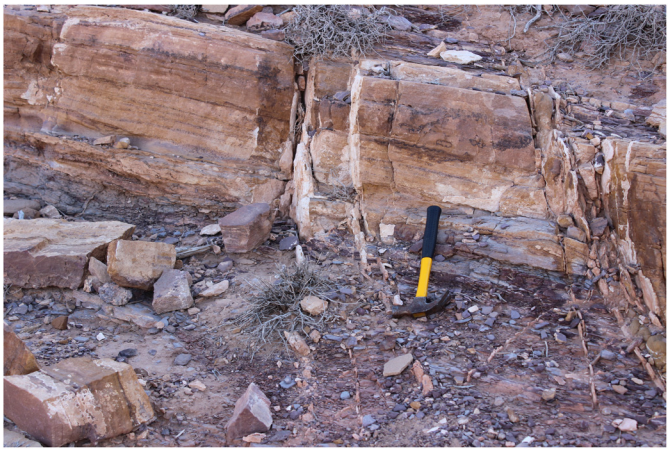

Fig. 5. Location WN2, where the carbonate veins penetrate from the underlying BQP rhyolite, an overlying shale layer and finally into the Salib Arkosic Sandstone.

an elevation of 960 m asl, the BQP crops out and continues all the way until the Quwayra fault.

The exposures of the BQP vary from fresh quartz feldspar porphyry to highly altered rock with notable stockwork carbonate veins within a fine-grained clayey matrix (Fig. 3). At elevation 960 m asl (point 1 in Fig. 1), the carbonate veins range from millimeter scale up to about 1 cm in thickness. The orientation of the veins varies, but with a dominant NS strike orientation (Fig. 4). A 30–40 cm soil overlies the altered BQP at this point. The clayey matrix in the altered zone contains greenish to yellowish oriented vein-like structures (cm scale thickness) as well. While at some limited places it looks like these clayey veins may have penetrated the BQP in a pressurized form, resulting in fissility of shale that aligns horizontally with the fracture pattern (sample taken and named WN7), this is clearly not the case with the carbonates, which show no brittle deformation. It is notable that many joints within the fresh outcrops at the site are devoid of alteration products and of carbonates. Juniper trees growing on such outcrops have roots that extend deeply into the fractures, with no evidence of alteration in these cases.

At the contact between the BQP and the overlying Abu Khushayba Sandstone near location 1 (location 2), a large vein of carbonate with a thickness reaching 7 cm penetrates a shale layer near the bottom of the sandstone formation into the formation. Here, the veins are thicker and more prominent, but not as numerous as those found at location 1 (Fig. 5). The orientation of the veins here is mostly at 60°.

About 100 m to the west of point 1, at location 3, the alteration zone is localized within the fresh BQP outcrop with carbonate veins reaching thicknesses of 5 cm within that zone (Fig. 6). The veins branch out from a main feeder here, which is notably thicker than the branches.

About 1.5 km to the north of point 1, point 4 shows similar alteration and carbonate formations. Here the alteration is wider and extends almost 200 m, with soil forming atop and an ancient valley fill at one location cutting though the alteration zone. The thickness of the carbonate veins here reach up to 2 cm, and there appears to be no preferred orientation for them.

Point 5 about 500 m to the east of point 4 is a localized alteration zone that contained notable moisture at the time of sampling (Sept. 5, 2014). This was toward the end of the long dry summer, and so was noted for that. The altered zone here has a reddish color, and the carbonates within it are in the form of horizontal pans reaching thicknesses of about 3 cm.

At about 8.5 km to the west of these points, to the west of the Quwaira fault, lies a small hand dug well at the margins of Wadi Araba known as Bir Mathkur (depth 4–5 m). This well lies at an elevation of 314 asl. Being to the west of the fault it straddles the deformed Upper Cretaceous rocks on the down faulted block to its east and the recent alluvial sediments in which it is dug. Ephemeral surface water drainage from the uplands converges from two tributaries converging from north and south at the well. Thus, water in the well comes from surface water infiltration within the permeable alluvium and perhaps from groundwater seeping from the highlands to the east, including both the immediate Upper Cretaceous limestones but also the BQP, which covers a significantly larger area and occupies the higher reaches of the escarpment

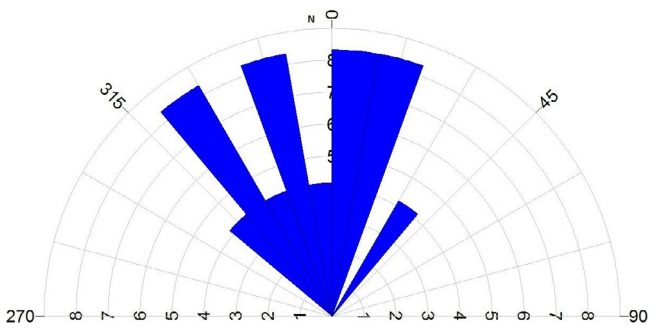

Fig. 4. Rose diagram of the orientation of the carbonate veins at WN 1, which follow the general structural trend of the region.

Fig. 6. Alteration zone at WN 3, with the feeder and branch veins clearly showing.

Table 1
Samples used in this paper.

Sample name	Source	Description	Minerals	Notes
WN1-F	Wadi Namaleh 1	Fresh Al Bayda QFP	Quartz, k-feldsar (sanidine), albite.	
WN1-A	Wadi Namaleh 1	Altered and friable rock in which secondary carbonates have grown.	Montmorillonite, sanidine, quartz, calcite.	
WN1-C	Wadi Namaleh 1	Carbonate vein sample	Calcite.	Thickness around 1 cm.
WN-2	Wadi Namaleh 2	Sample from carbonate vein.	Calcite.	Carbonate vein extending from the altered rhyolite to the overlying Palaeozoic sandstone. Thickness reaching 7 cm.
WN3-F	Wadi Namaleh 3	Fresh Al Bayda QFP	Quartz, feldspar, albite.	
WN3-A	Wadi Namaleh 3	Altered and friable rock in which secondary carbonates have grown.	Montmorillonite, sanidine, quartz, calcite.	
WN3-C	Wadi Namaleh 3	Carbonate vein	Calcite.	Thickness around 5 cm.
WN5-A	Wadi Namaleh 5	Altered and friable rock in which secondary carbonates have grown.	Montmorillonite, sanidine, quartz, calcite.	Moist at sampling. Tree growing above.
WN5-C	Wadi Namaleh 5	Carbonate vein in moist altered material.	Calcite.	Reddish in color. Around 3 cm.
WN-7	Wadi Namaleh 7	Deformed shale material near Wadi Namaleh 1	Kaolinite, montmorillonite and quartz	Reddish with green streaks

where most of the precipitation falls. Water from this well can help constrain the range of isotopic contents in waters from the upper highland rainwaters down to Wadi Araba to the west.

2. Materials and methods

Samples of fresh quartz feldspar porphyry, its alteration products and the intergrown carbonate were collected from sites 1, 3, 4 and 5 described above. A sample from the carbonate veins at site 2 was also collected for later mineralogical, geochemical, isotopic and textural analysis. Water samples were also collected from Bir Mathkour for chemical and isotopic analysis in the late winter (February 25, 2015).

The solid samples were analyzed for major elements using inductively coupled plasma optical emission spectrometry (ICP-OES) model Perkin Elmer Optima 7000 DV. This device is housed at the Jordan Atomic Energy Commission. The silicate samples (the fresh rock and altered material) were totally dissolved in an aqua regia solution, whereas the carbonate samples were dissolved in analytical grade HCl in order to exclude silicate traces from the results. A similar approach was taken in digesting the samples for strontium isotopes. Rare Earth Elements and other trace metals (30 elements) were determined using Neutron Activation Analysis at Bonn University after subjecting the samples to a neutron flux for 10 h (flux 5×10^{12} neutrons/cm^2/sec) at the Reactor Institute at Delft, The Netherlands, according to the method described by Mommsen et al. (2016).

The mineralogy of the fine-grained particles of the alteration products was determined using a Shimazo X-Ray diffractometer housed at Yarmouk University in Irbid, Jordan. The desired fine fraction was separated in water using a settling tube. The unoriented samples were scanned from 4° to 60° using CuKα radiation with 30 kV, 30 mA energy and graphite monochromater. Minerals were manually identified using JCPDS Card data.

Petrographic thin sections for fresh and altered rhyolite (location 3) were produced in the geology laboratories of the Hashemite University, and the petrography was studied using a Leica DM750 microscope at the German Jordanian University.

Scanning electron microscopy (SEM) was conducted at Yarmouk University using an FEI Quanta 200 with an attached energy dispersive x-ray attachment for small scale elemental analysis. Samples were gold-plated for this purpose.

The $^{87}Sr/^{86}Sr$ ratios were measured for the fresh and altered rocks as well as for the carbonates at the Saskatchewan Isotope Laboratory at the University of Saskatchewan, Canada. The carbonate samples were dissolved from the silicate matrix to ensure that the results represent only the carbonate, whereas the fresh and altered rhyolite were dissolved as whole-rock samples. Carbonate samples (~0.50 g) were dissolved by addition of 0.5 N HCl until the effervescence ceased in Teflon "Savillex" beakers. The silicate samples (~150 mg) were dissolved using a mixture of concentrated HF (5 ml) and concentrated HNO_3 (3 ml) acids in Savillex TM Teflon screw-top vials in an oven for 3 days at 130 °C. Sr was purified from matrix elements using Bio-Rad AG50Wx12 (200–400 mesh) cation exchange resin with elution in HCl. $^{87}Sr/^{86}Sr$ ratios were determined by thermal ionization mass spectrometry on a Thermo Fisher Triton instrument using static multicollection. The measured $^{87}Sr/^{86}Sr$ ratios were normalized to a value of 0.1194 for $^{87}Sr/^{86}Sr$. The relative external precision of the analyses is better than ±12 ppm, based on repeat analyses of samples and standards. During the course of this work the NIST 987 standard yielded 0.710276.

Carbonate samples were analyzed for stable carbon and oxygen isotopes at the Friedrich Alexander Universitat in Erlangen, Germany. The carbonate powders were reacted with 100% phosphoric acid at 70 °C using a Gasbench II connected to a ThermoFinnigan Five Plus mass spectrometer. Results were reported in per mil versus PDB.

The stable isotopic composition of the water from Bir Mathkour (O, H and C) was measured at the Water Authority of Jordan laboratories. The oxygen and hydrogen isotopes were determined using a Finnigan Matt Delta PlusXPlHDO mass spectrometer (with Pt). The dissolved carbonate carbon isotope content was measured using a CRDS analyzer using the same mass spectrometer.

3. Results

The sources of the samples and their mineral compositions, as determined by XRD are listed in Table 1. The samples are characterized as "fresh", meaning that they consist of pristine appearing hard country rock; "altered", meaning that they consist of soft, friable clayey material and carbonate. The fresh samples show the expected composition for the dominant BQP of the area (Barjous, 2003). The altered silicate fraction is dominated by montmorillonite (or mixed layer illite/montmorillonite) in addition to the primary minerals present in the BQP (quartz and sanidine) and calcite (Fig. 7). The carbonate samples consist of calcite.

Petrographic examination of the unaltered sample of BQP shows a quartz-rich fine groundmass with larger phenocrysts of quartz

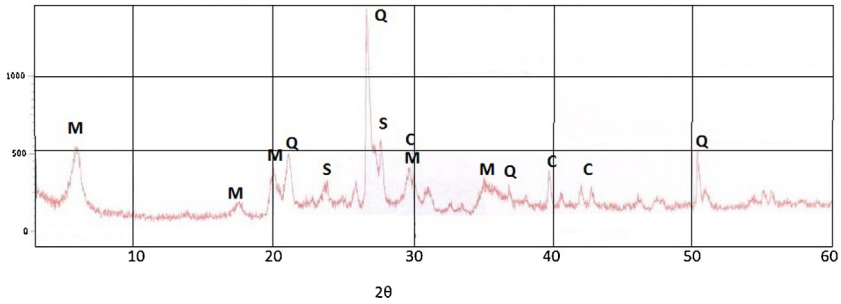

Fig. 7. XRD pattern for the clay fraction from the altered zone at location 3 (CuKα). Distinctive montmorillonite (M), quartz (Q), sanidine (S) and calcite (C) are seen.

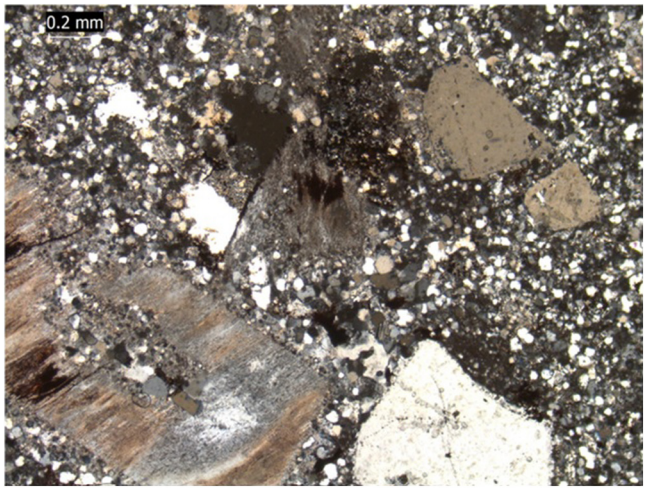

Fig. 8. Petrographic image of fresh BQP showing perthite phenocrysts in a fine grained quartz and feldspar matrix. XPL.

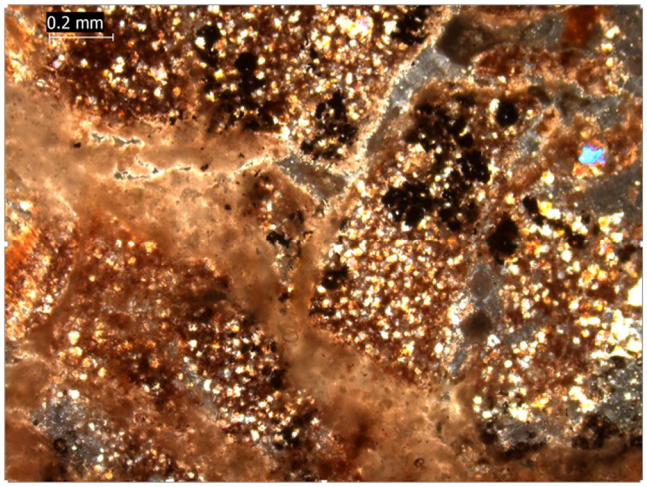

Fig. 9. Petrographic image of altered BQP showing carbonate veinletts penetrating both the fine grained matrix on the right and the large phenocryst on the left. XPL.

and feldspar, some of which is showing perthitic texture (Fig. 8). The altered samples of BQP show their alteration in thin section in the form of extensive calcite growth both within and between the various grains present within the mother rock, not following the intergranular boundaries (Fig. 9). The SEM analysis focused on the nature of the alteration products in terms of textural relationships. The carbonate grains are notably very fine (micrometer to ten micrometer scale; Fig. 10). Both the primary grains of sanidine and quartz seem to be coated with alteration products, with little evidence to deep transitional alteration zones (Fig. 11). In some cases, progressive fronts of alteration can be seen, although the intersection of altered and unaltered phases remains clear (Fig. 12). Recrystallization of calcite can be discerned in some cases as well (Fig. 13). Energy dispersive X-ray fluorescence spot analyses (standardless) suggest that the clay fraction is montmorillonite (with an Al:Mg atomic ratio of between 1:1 and 1:3), with some evidence of illite montmorillonite mixed-layers (with traces of K) in some cases. Thus, both dioctahedral and trioctahedral montmorillonite seem to be present. The mineralogical analysis shows no evidence of kaolinite.

The results of the major element analysis of the solid samples are presented in Table 2. The data for the fresh samples are consistent with rhyolite (Le Maitre, 1984). The altered products,

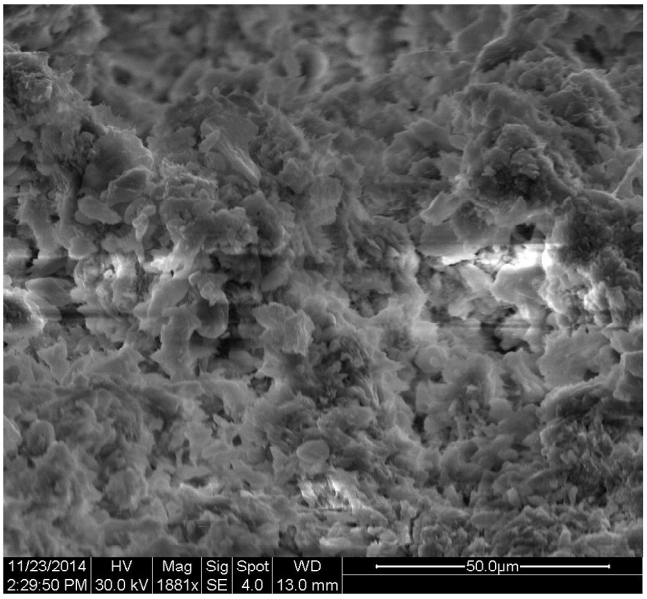

Fig. 10. Alteration products at WN 1 under SEM, showing fine grained calcite growth.

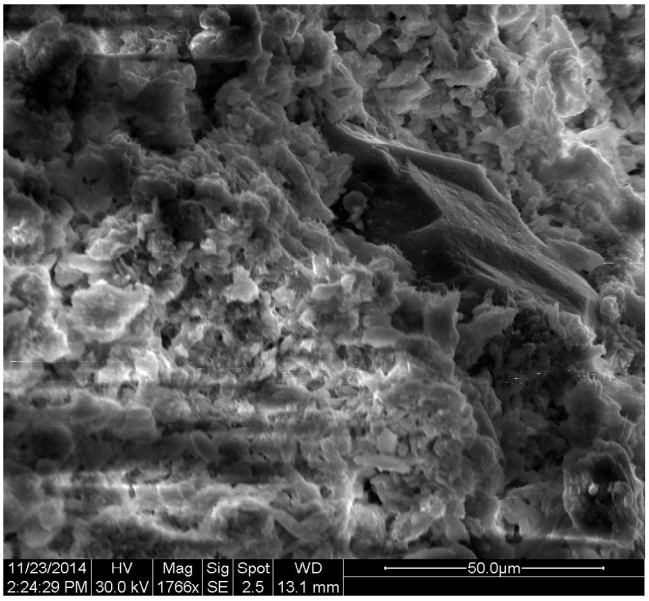

Fig. 11. Alteration products from WN 4 under SEM showing clay and calcite alteration products, and a very fresh quartz grain.

shown previously to consist of montmorillonite (or mixed layer illite-montmorillonite), in addition to the primary minerals and secondary calcite, is reflected in the major chemistry of the samples where there is a loss in silica, a gain in calcium and a slight gain in the magnesium contents within the altered samples. Most of the missing mass in the oxide totals is probably CO_2 or H_2O. There is a clear negative correlation between aluminum and calcium concentrations (Fig. 14), which in sharp contrast to the positive correlation between aluminum and iron and aluminum and potassium (Fig. 15).

The Rare Earth Element (REE) composition of the samples are presented in Table 3 and normalized REE patterns in Fig. 16. These show that Eu-depleted signature of the fresh rhyolite is constant through the altered and carbonate samples as well. Two exceptions are the clay from WN7, which shows no Eu anomaly, and the

Table 2
Major chemical constituents in the analyzed samples. Samples with the letter D at the end are duplicates.

Sample	Al_2O_3 (%)	SiO_2 (%)	Fe_2O_3 (%)	CaO (%)	MgO (%)	Na_2O (%)	K_2O (%)	Total (%)
WN1-A	6.34 ± 0.14	55.14 ± 1.22	2.09 ± 0.04	9.98 ± 0.24	1.67 ± 0.03	0.21 ± 0.01	3.84 ± 0.10	79.27
WN1-A (D)	6.54 ± 0.07	58.45 ± 0.56	2.10 ± 0.03	10.05 ± 0.15	1.64 ± 0.02	0.22 ± 0.01	3.98 ± 0.05	82.98
WN3-A	8.48 ± 0.12	71.14 ± 1.15	3.06 ± 0.02	2.06 ± 0.04	1.00 ± 0.00	0.39 ± 0.01	5.37 ± 0.13	91.50
WN5-A	7.31 ± 0.12	61.71 ± 0.65	2.43 ± 0.02	8.86 ± 0.16	1.16 ± 0.01	1.10 ± 0.01	5.17 ± 0.04	87.74
WN1-F	7.38 ± 0.22	74.34 ± 2.72	5.36 ± 0.17	0.49 ± 0.01	0.59 ± 0.01	2.09 ± 0.08	5.68 ± 0.11	95.93
WN3-F	9.49 ± 0.69	74.72 ± 7.02	4.49 ± 0.31	1.33 ± 0.10	0.67 ± 0.06	1.42 ± 0.06	7.83 ± 0.31	99.95
WN1-C	1.00 ± 0.02	0.88 ± 0.03	0.25 ± 0.01	31.78 ± 0.57	3.61 ± 0.09	0.15 ± 0.01	0.08 ± 0.00	37.75
WN1-C (D)	1.02 ± 0.01	0.27 ± 0.02	0.24 ± 0.01	34.98 ± 0.43	3.69 ± 0.06	0.18 ± 0.00	0.09 ± 0.00	40.47
WN3-C	0.93 ± 0.01	0.00 ± 0.00	0.23 ± 0.01	42.72 ± 0.63	0.55 ± 0.01	0.12 ± 0.00	0.07 ± 0.00	44.62
WN5-C	0.38 ± 0.01	0.00 ± 0.00	0.30 ± 0.01	39.67 ± 0.60	0.92 ± 0.01	1.00 ± 0.02	0.07 ± 0.00	41.23

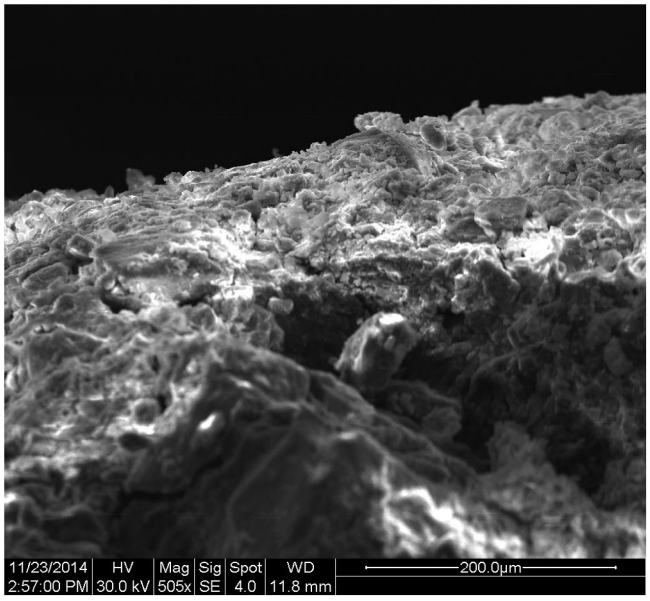

Fig. 12. Alteration and calcite deposition at WN4. The fresh looking feldspar grain the foreground shows slight alteration at the cleavage planes and at microcracks within the grains.

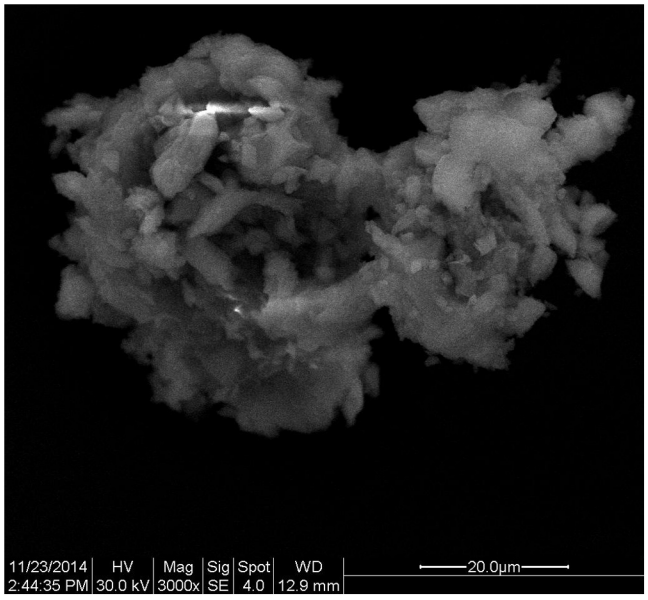

Fig. 13. Recrystallization of calcite seen in the veins of WN5.

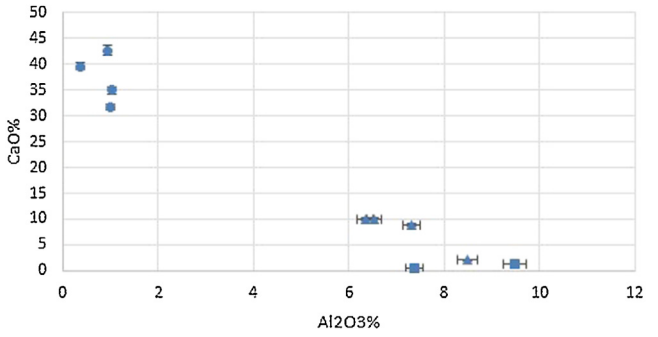

Fig. 14. Scatter diagram of the Al_2O_3 and CaO contents of the analyzed samples. Circles are carbonate, squares are fresh rhyolite and triangles are altered rhyolite.

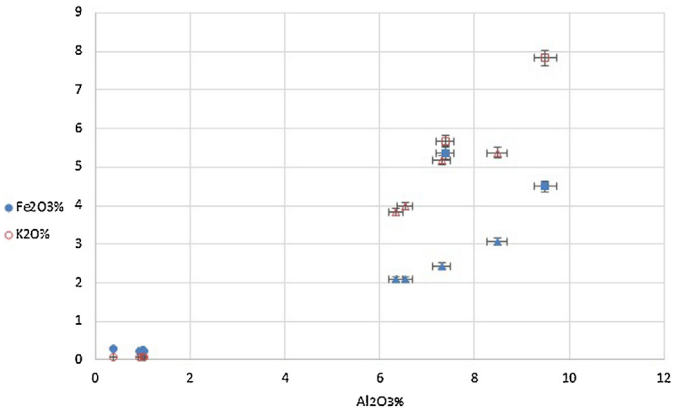

Fig. 15. Scatter diagram of the Al_2O_3 versus K_2O and Fe_2O_3 in the analyzed samples. Circles are carbonate, squares are fresh rhyolite and triangles are altered rhyolite.

carbonate sample from WN2, which also has no Eu anomaly and a notably low REE content generally.

Other trace element results are presented in Table 4. The most obvious trend seen here is the lower metal contents in the carbonate veins than in the fresh or altered rhyolite samples. Carbonate tends to be a poor host for trace metals, and thus this observation is not surprising. Nickel concentrations are below detection limits in the fresh rhyolite, but measurable in the altered rhyolite and in the carbonates.

The trends related to both major and trace elements show that most pH and Eh sensitive metals maintain the same ratios between the three sample types. For example, the correlation between the largely insoluble aluminum and iron and potassium is shown in Fig. 15. This figure seems more likely to represent dilution of all the components presented (mostly by CaO), rather than any significant leaching. Heavy metals like arsenic do not show any strong trends of mobility, as can be seen in Fig. 17.

Table 5 shows the results of the stable isotope analyses for carbon and oxygen in the carbonate samples. The stable carbon $\delta^{13}C$

Table 3
Rare earth element contents in the samples (in ppm).

Sample	La	Ce	Nd	Sm	Eu	Tb	Yb
WN1-F	52.5 ± 0.14	135 ± 0.48	53.7 ± 3.39	9.35 ± 0.31	0.54 ± 0.014	1.32 ± 0.068	4.79 ± 0.056
WN4-F	108 ± 0.11	260 ± 0.43	112 ± 3.13	21.8 ± 0.92	1.27 ± 0.011	3.03 ± 0.096	9.18 ± 0.063
WN1-W	79.6 ± 0.084	160 ± 0.22	86.3 ± 3.07	14.9 ± 0.39	0.83 ± 0.008	2.04 ± 0.047	7.12 ± 0.05
WN3-W	58.8 ± 0.12	108 ± 0.39	63.5 ± 3.03	11 ± 0.32	0.62 ± 0.012	1.51 ± 0.051	4.92 ± 0.078
WN5-W	45.4 ± 0.17	101 ± 0.66	44.5 ± 5.98	9.88 ± 0.35	0.78 ± 0.017	1.34 ± 0.054	4.58 ± 0.055
WN1-C	34.2 ± 0.008	23.9 ± 0.15	36.6 ± 2.31	4.44 ± 0.3	0.19 ± 0.006	0.29 ± 0.017	0.74 ± 0.027
WN2-C	0.77 ± 0.07	3.4 ± 0.39	1.15 ± 0.86	0.25 ± 0.052	0.055 ± 0.013	0.041 ± 0.013	0.071 ± 0.014
WN3-C	49.2 ± 0.071	119 ± 0.36	48.9 ± 2.41	11.4 ± 0.36	0.69 ± 0.014	1.83 ± 0.042	6.32 ± 0.059
WN7	70 ± 0.089	110 ± 0.37	56.3 ± 2.38	7.34 ± 0.17	0.55 ± 0.013	0.33 ± 0.025	1.2 ± 0.034

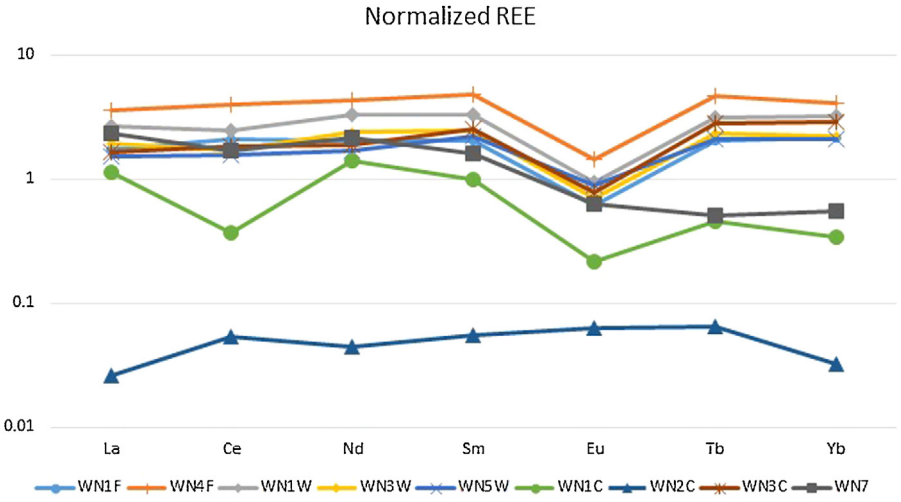

Fig. 16. REE normalized to North American Continental Crust, based on Taylor and McLennan (1985).

Table 4
Selected trace metals in the studied samples (in ppm).

Sample	Ni	As	Sb	W	Ba	U
WN1-F	na	12.3 ± 0.15	1.2 ± 0.025	0.77 ± 0.2	161 ± 24.7	2.31 ± 0.19
WN4-F	na	8.32 ± 0.16	0.73 ± 0.026	1.57 ± 0.22	172 ± 26.6	6.06 ± 0.23
WN1-W	18.6 ± 13.8	13.7± 0.14	1.7 ± 0.025	1.27 ± 0.17	310 ± 22.7	4.81 ± 0.19
WN3-W	27 ± 11.9	9.18 ± 0.12	0.87 ± 0.02	0.90 ± 0.15	222 ± 19.2	2.85 ± 0.16
WN5-W	47 ± 11.4	3.65 ± 0.07	0.29 ± 0.023	1.00 ± 0.09	69.8 ± 37	1.57 ± 0.17
WN1-C	64.5 ± 8.3	4.17 ± 0.087	0.092 ± 0.013	0.32 ± 0.1	98 ± 14.7	0.76 ± 0.11
WN2-C	138 ± 8.8	0.96 ± 0.02	0.035 ± 0.006	0.22 ± 0.023	170 ± 10.8	0.084 ± 0.046
WN3-C	64.9 ± 11.7	8.02 ± 0.058	0.69 ± 0.017	0.47 ± 0.057	122 ± 25.2	2.34 ± 0.13
WN7	15 ± 12.4	9.67 ± 0.06	0.27 ± 0.015	0.79 ± 0.057	92.5 ± 22.8	1.63 ± 0.13

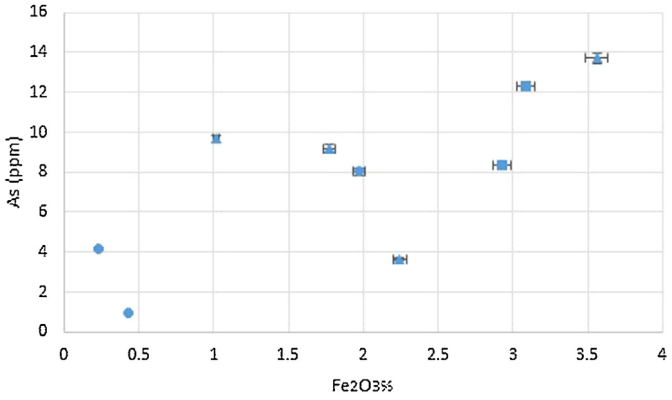

Fig. 17. A scatter diagram showing the relationship between Fe_2O_3 and As. Circles are carbonate, squares are fresh rhyolite and triangles are altered rhyolite.

Table 5
Stable isotope contents in the carbonate samples.

Sample ID	$\delta^{13}C$ ‰ VPDB	$\delta^{18}O$ ‰ VPDBcalcite
WN 1	−7.31	−3.93
WN 2	−7.82	−5.53
WN 3	−9.48	−4.08
WN 5	−7.95	−3.77

signature ranges from −7.3 to −9.5 per mil versus PDB. The oxygen $\delta^{18}O$ signatures range from −3.8 to −5.5 per mil versus PDB.

Table 6 shows the results of the $^{87}Sr/^{86}Sr$ ratio analysis. These show that there is a clear distinction between the fresh ($^{87}Sr/^{86}Sr = 0.885161$ for sample WN-1 F) and altered host rhyolite ($^{87}Sr/^{86}Sr$ between 0.719418 and 0.739092) and the carbonates within them ($^{87}Sr/^{86}Sr$ between 0.708388 and 0.708434).

The isotopic characteristics of the water of Bir Mathkour are presented in Table 7.

Table 6
Results of Sr isotope analyses.

Sample	$^{87}Sr/^{86}Sr$	2 s.e.
WN1 F	0.885161	0.000025
WN1-A	0.739092	0.000005
WN1-C	0.708434	0.000005
WN 2	0.708388	0.000005
WN 7	0.719418	0.000006

Table 7
Isotopic analysis of water of Bir Mathkour. Oxygen and hydrogen isotopes are in per mil units versus VSMOW. The carbon represents the dissolved carbonate in the water and is represented in per mil PDB.

Sample	δD	$\delta^{18}O$	$\delta^{13}C$
Bir Mathkour	−27.49	−5.83	−7.94

4. Discussion

The conditions under which the alteration and vein deposition have occurred are important for the question of the ultimate fate of leaking CO_2 from CCS reservoirs. Studies of magnesite hosted in ultramafic rocks have shown deposition in two ways. Deeply formed massive magnesite, associated with talc formation and more shallow magnesite in the form of veins embedded in near-surface alteration zones (Abu-Jaber and Kimberley, 1992a). While there are visual similarities existing between the calcium carbonates seen in Wadi Namaleh and the shallow magnesite deposits described in the past, these are not enough to draw any correlations between these phenomena.

The field relationships at Wadi Namaleh support the notion that the carbonates and the alteration zones were produced at the same time. The two features occupy the same spaces and are extremely intermingled, and are never seen separated from each other, with the exception of the carbonate veins in the sandstone, which has no aluminosilicates to weather into clay. Thus, it is safe to assume that the two are cogenetic in time and in formation process. Field relationships also contain a number of other notable clues on the genesis of these carbonate veins and associated alteration zones. For example, not all of the fractures in the BQP rhyolitic porphyry are associated with alteration or with carbonate deposition. Moreover, while the alteration zones seem to be confined to the near-surface, not all of the near-surface areas contain evidence of alteration. Additionally, most of the alteration zones seen are overlain by immature soil and/or colluvium. Most of the colluvium that overlay the alteration zones are only a few centimeters thick. Joint sets that are uncovered by soil or colluvium are almost always fresh with no evidence of alteration, even with the growth of trees and shrubs in them.

The presence of alteration zones only when there is a soil cover does not seem to be a coincidence, although it could be argued that the soil is formed from organic activity within the upper part of the alteration zone. This, however, would imply that CO_2 is only leaking from specific joints or joint sets, thus limiting soil formation to specific areas. This does not seem to be plausible, given that there seems to be no preferred joint set (besides the predominant jointing pattern in the area), where the carbonate is deposited, and the abundance of horizontal carbonate pans which follow no tectonic pattern.

Trees and shrubs growing in the area are also occasionally associated with the presence of alteration zones, but in many cases roots seem to extend deeper into the unaltered hard rock with no visible resulting alteration associated with that.

The soft altered zone in some limited places (WN-7) seems to have been extruded under pressure, but this appears to be local, and as noted previously none of the associated carbonate seems to have undergone flow or any brittle deformation. The REE patterns associated with this zone suggest that it comes from a different source, and not derived from the local mother rock (Fig. 16).

Thus, these field relationships do not support any contention that the alteration zones or carbonate deposits are normal weathering phenomena or related to simple surficial processes. The presence of veins that penetrate into the overlying sandstone at WN-2 (Fig. 5) bears this conclusion out.

The fresh rhyolite dominating the area is not surprising, given the active tectonics and arid climate. The extent of alteration within the alteration zones is remarkable, especially when contrasted with the adjacent unaltered BQP material, which is very fresh. The altered zones indicate that anomalous conditions have been at work. The association of the carbonate veins with them suggest a strong genetic relationship.

The chemistry of the major elements are within the expected ranges in all types of samples. In looking at CaO/Al_2O_3 ratios, which reflect changes in the CaO relative to an immobile metal (Al_2O_3), it is clear that the CaO has been enriched during alteration (Fig. 14). This is probably a reflection of the growth of secondary calcite (Fig. 9), but provides little insight into the source of the calcium. There is also a modest enrichment in MgO. Table 8 is a correlation matrix for the major elements within the analyzed samples. A strong positive correlation is seen between Al_2O_3, Fe_2O_3, and SiO_2, and a strong negative correlation is seen between Al_2O_3 and CaO. Na_2O and MgO are interesting here because they don't correlate well with the fresh silicate or the carbonate end members, and thus reflect the degree of alteration leading to the formation of illite/montmorillonite.

The REE and the metals seem to be mostly immobile in this context, with no evidence of leaching or fractionation related to the alteration process. Two conclusions can be drawn from this. The first is that the process does not seem to involve significant input of exotic metals (save calcium and perhaps magnesium), and the second is that no redox processes seem to be at work, given the REE patterns seen. Under reducing conditions, trivalent Eu tends to change into the divalent form (Brookins, 1989). From the examination of the REE patterns shown in Fig. 15, it is clear that the negative Eu anomaly is a relic of a similar anomaly present in the fresh rhyolite. Two samples do not follow this pattern. The aforementioned WN7, which seems to have been extruded from adjacent rock formations rather as a local alteration product, and WN2-C, which is a carbonate sample penetrating into the overlying sandstone (Fig. 5). Not only is WN2-C free of any rhyolite REE signatures, but it has notably low absolute REE concentrations. All of these data suggest

Table 8
Correlation matrix of the major elements in the analyzed samples.

	Al_2O_3	CaO	K_2O	Fe_2O_3	MgO	Na_2O	SiO_2
Al_2O_3	1						
CaO	−0.97607	1					
K_2O	0.984052	−0.95465	1				
Fe_2O_3	0.884615	−0.90554	0.925009	1			
MgO	−0.48653	0.380881	−0.52895	−0.54505	1		
Na_2O	0.46306	−0.49455	0.584718	0.759059	0.54391	1	
SiO_2	0.964874	−0.95102	0.98957	0.96075	0.53075	0.630219	1

that REE and other metals did not become significantly mobilized during the alteration process, even for the few meters it would have needed to move from the rhyolite to the carbonate vein in the adjacent sandstone. For significant mobilization, movement of a CO_2-charged, saline or heated water is needed (Ueda et al., 2005; Little and Jackson, 2010; Holzheid, 2016, among others), which is evidently not the case here.

The development of montmorillonite (or illite/montmorillonite) here is also of interest. Phase diagrams showing conditions of montmorillonite formation were presented by Garrels (1984), illustrating the nature of phase transition from feldspar to montmorillonite (and illite) to kaolinite to gibbsite. These are more related to the concentration of the silica in the fluid than to the $a(K^+/H^+)$, implying a relatively limited pH control over the process, with the presence of silica-poor water as being the key factor. The genesis of the silicate alteration products seem to be functions of CO_2-water interaction with the parent rock (Fischer et al., 2010), whereas the CO_2 and its effect on pH more closely controls the calcite precipitation. Both processes need water to stay in place long enough for the reactions to proceed. It is interesting to note that the alteration of serpentinite in Margarita Island, Venezuela through CO_2 charged water leads to the formation of nontronite, an iron-rich smectite (Abu-Jaber and Kimberley, 1992b). Similarly, alteration of basalt in northeastern Jordan leads to the formation of montmorillonite and nontronite. It has been suggested by Kimberley and Abu-Jaber (2005) that a positive feedback mechanism is working there, with the clay formation acting to trap water and CO_2, thus increasing the efficiency of the process.

The stable carbon isotopes in the calcite veins show a notably light signature. The most effective way for carbon isotope fractionation is through photosynthesis. Thus, terrestrial pedogenic carbonates show signatures that reflect soil CO_2 derived from decaying organic material (Cerling, 1984). Quade et al. (1989) have shown that such pedogenic carbonates vary in isotopic composition according to altitude at climate, with the lightest signatures (about -5‰ $\delta^{13}C$ PDB) characteristic of areas with higher elevation (1900 m) and predominance of plants using C3 photosynthetic pathways. Moreover, low soil CO_2 and contact with the atmosphere contents tend to lead to have enriched $\delta^{13}C$ values. It is clear that the Wadi Namaleh carbonates have notably lighter $\delta^{13}C$ values, despite falling at a significantly lower elevation with an arid climate, as is shown in Table 3, which suggests a different carbon source. Calcretes in the West Bank formed through organic/atmospheric sources of carbon have notably heavier isotopic signatures (Sokol et al., 2014).

Eraifej (2006) reported $\delta^{13}C_{CO2}$ values from deep wells along the Jordan Valley of between −16.9 to −22.9 $\delta^{13}C$ PDB. As noted previously, the $\delta^{13}C$ for the CO_2 is in disequilibrium with the reported $\delta^{13}C$ for the dissolved bicarbonate in the same samples (ranging from −4.1 to −12.1‰ PDB), leading to the conclusion that an extraneous source exists for this carbon. The stable carbon signatures of the various potential carbon sources and authigenic carbonates in the region are shown in Fig. 18.

Carbon isotopic equilibrium relationships in water were first investigated by Deuser and Degens (1967). They found that there is isotopic fractionation as a result of CO_2 being in contact with water. This fractionation is temperature dependent and occurs when the CO_2 is hydrated to H_2CO_3. Subsequent work by Zhang et al. (1995) has resulted in a better understanding of the fractionation relationships involved. This has been formulated as follows:

$$\varepsilon_{HCO_3-CO_2} = -(1.41 \pm 0.003)T(^\circ C) + (10.78 \pm 0.05)\,‰$$

(Zhang et al., 1995).

where $\varepsilon_{HCO3\text{-}CO2}$ is the per mil fractionation and T is temperature.

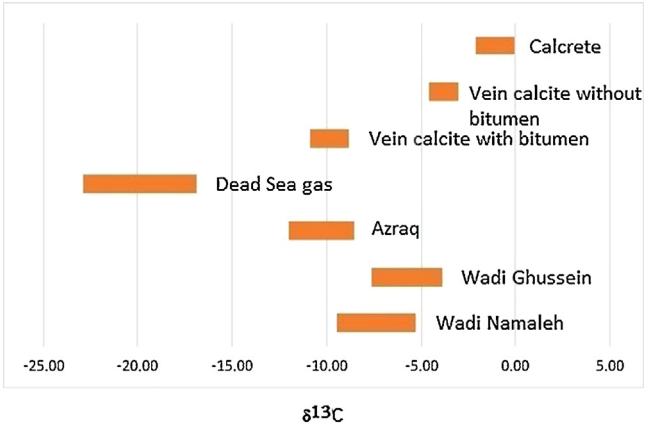

Fig. 18. The ranges for carbon stable isotopic contents for various authigenic carbonates and deep carbon sources in Jordan. Calcrete, vein calcite without bitumen and vein calcite with bitumen are from Sokol et al. (2014); Dead Sea gas is from Eraifej (2006); Azraq dissolved carbon from Kaudse (2014); Wadi Ghussein from Kimberley and Abu-Jaber (2005) and Wadi Namaleh (this study).

Solving this equation for T using the data presented by Eraifej (2006) yields temperatures of 16–21 °C. Since direct measurements of these well waters show temperatures ranging from 35 to 48 °C, it is clear that the CO_2 is not in equilibrium with the HCO_3^- dissolved in the water.

This anomaly can be explained in two ways. The first and most obvious is that there is another source of carbon. Because atmospheric carbon is markedly heavier (−7.4‰ PDB). The second is that the dissolved carbonate is undergoing a second fractionation event by way of degassing. Data presented by Kaudse (2014) only show the $\delta^{13}C$ of the dissolved carbonates from the Jordan Valley and Azraq wells. As there is no isotope data for the accompanying gases, it is difficult to assess very much beyond the sources of the coexisting carbon sources. Some of them are similar to those reported by Eraifej (2006), while others are significantly more enriched in ^{13}C. The dissolved carbon isotopes reported by Inguaggiato et al. (2016) are similar to those of Kausde (2014).

Calcite precipitation involves little fractionation in carbon isotopes (Romanek et al., 1992). Thus the $\delta^{13}C$ signature for the carbonates reflects about a 1‰ enrichment from the solution from it precipitates from, with no temperature dependence.

The $\delta^{13}C$ values in the vein carbonates of Wadi Namaleh range from −7.3 to −9.48‰ PDB. It is noteworthy that the dissolved carbonate in the Bir Mathkour water was −7.94‰, and thus falls within the range of the carbonates in the area. The distance, elevation difference and geological variability between Bir Mathkour and the alteration zones in Wadi Namaleh argue against similar processes occurring at both sites. This does not preclude both sites experiencing similar carbon leaking and rainwater isotopic compositions. Thus, while the Bir Mathkour water is not directly involved in the precipitation of carbonate, it does seem to show some of the chemical and isotopic fluxes that are present in the area. For example, the oxygen and hydrogen isotopes clearly reflect modern rainwater in the region (see Bajjali and Abu-Jaber, 2001). Carbonate veins formed in the basalt fields of northeastern Jordan are similarly depleted in ^{13}C, but slightly less so than in the carbonates of Wadi Namaleh (Kimberley and Abu-Jaber, 2005).

Oxygen isotopic values are generally heavy for rainwaters, groundwater (Bir Mathkour) and calcite veins. Assuming that the calcite precipitated in equilibrium with meteorically-derived local waters, it is possible to calculate the temperature of precipitation in accordance with the relationship derived by Kim and O'Neil (1997): $1000\ln\alpha(\text{Calcite-}H_2O) = 18.03(10^3\,T^{-1}) - 32.42$ where α is

the oxygen isotopic fractionation between the calcite and the water, and T is the temperature in degrees Kelvin.

Solving for temperature using the available well water at Bir Mathkour and the carbonate oxygen isotope data yields precipitation temperatures of between 5 and 13 °C. As these temperatures are slightly lower than expected, given that the ambient temperature in the area is about 20 °C, it is possible that evaporated waters with heavier isotopic ratios (about −3‰ VSMOW) are responsible. Such water might be found in the moist zone noted at WN-5.

It is noteworthy that both the carbon and oxygen isotopes suggest that the carbonates within the altered zones of the BQP were formed under ambient near-surface conditions, as is suggested by the field relationships. These corroborate the conclusions derived from the study of the REE and the trace metals at the site, i.e. the temperature was ambient.

Contrasting the carbonate veins at Wadi Namaleh with the veins described by Sokol et al. (2014) reveals that the carbon and oxygen isotope ratios in Wadi Namaleh are similar to those on the West Bank, specifically the carbonates associated with bitumen there. On the other hand, Wadi Namaleh carbonates are notably lighter in oxygen and carbon than their bitumen-free counterparts on the West Bank. Despite this, it is difficult to imagine that the bitumen embedded carbonates described by Sokol et al. (2014) are genetically related to the carbonates at Wadi Namaleh, given the totally different geology of the two areas. The Cretaceous outcrops in the down faulted areas to the west only expose the sequences that underlay the bitumen-bearing Muwaqqar Chalk Marl formation (Barjous, 2003). Pedogenic carbonates reported by Sokol et al. (2014) show distinctively heavier carbon isotopic signatures (Fig. 18).

The results of the strontium isotopes clearly show that the calcium within the carbonates is not derived from the BQP rhyolite. Extraneous sources of calcium can be envisioned to come along with the CO_2 in dissolved form, or with the supposed runoff or rainwater that is in isotopic equilibrium with the carbonates. Strontium isotopes are ideal tracers for the sources of calcium given the geochemical similarities between the two alkali earth elements, and thus are often used in that way (Van der Hoven and Quade, 2002; Castorina and Masi, 2015). The strontium isotopic signature of the altered host rock is intermediate between the fresh BQP rhyolite and the carbonate veins, which strongly suggests that it represents a mixture of the two components. Thus, the question arises regarding the source of the strontium (and calcium) in the carbonates.

Rainwater directly to the west of the study area in the Negev of southern Israel as well as the rest of the country was analyzed for chemical composition and strontium isotopes by Herut et al. (1993). The $^{87}Sr/^{86}Sr$ ratios of the Negev range from 0.70792 and 0.7084, which overlaps with the Wadi Namaleh carbonates. Mass balance modeling by Herut et al. (1993) would suggest that the dominant source of strontium in the rain water is dust derived from the Mesozoic and Cenozoic limestone formations in the region and beyond.

The flux of dissolved solids in the region is small compared to the flux of suspended solid dust. The flux of salts from precipitation in the Negev has been measured to be about 8 g/m^2 (Yair et al., 1991). On the other hand, dry deposition has been estimated in the Negev to be between 150 and 200 g/m^2 (Ganor and Foner, 2001). The composition of the dust varies according to grain size, with the coarse silt fraction makes up about 80% of dust deposits following dust storms in the eastern Mediterranean, and is dominated by calcite (~50%), followed by quartz (~40%) and feldspar (~10%; Ganor and Mamane, 1967). The clay-sized fraction is 13–40% clay minerals, 35–62% carbonates and 13–27% quartz (Ganor and Mamane, 1967).

Data on the Sr isotopic composition of the dust in the area is limited. Weldeab et al. (2002) studied surficial sediments of the Mediterranean Sea, and showed that the Saharan sourced aeolian input tended to show progressive lowering of $^{87}Sr/^{86}Sr$ toward the eastern Mediterranean. The farthest eastern sample off the coast of Israel had a ratio of 0.707531. The extensive review of the mineralogical and chemical characteristics of Saharan dust conducted by Scheuvens et al. (2013) did not reveal any other relevant information on this. Thus, it is assumed that since the data presented by Weldeab et al. (2002) is in agreement with the rainwater data presented by Herut et al. (1993), these represent a reasonable reflection of atmospheric input signatures, whether wet or dry.

Given that the strontium isotopic ratios in the Wadi Namaleh carbonate veins are within the range of the atmospheric input functions of the region, it is deduced that the source of the strontium and calcium in these veins is the remobilization of dry and wet atmospheric deposition in the region.

While clay, and most significantly montmorillonite, is a minor component in the aeolean deposition in the eastern Mediterranean (Ganor and Mamane, 1967), there is little evidence to deduce that the clays in which the carbonates veins are found are exotic, except for the extruded clay at WN-7. The field relationships and the SEM images discussed earlier show no evidence of aeolian deposition or transport through the joint systems of the BQP rhyolite. The overlying colluvium is obviously distinct from the underlying alteration zones of the rhyolite. In addition, the volume of the alteration product clay material exceeds that of the carbonate, which is not the case of the dust itself.

5. Conclusions

A general explanation of the model deduced herein is presented in Fig. 19. The near-surface alteration horizon reflects an interaction zone between the atmospheric input of water and calcium, in addition to quartz and clay, and a deep sourced CO_2 flux. This interaction leads to the formation of montmorillonite clay and calcite. This occurs under ambient near surface conditions with no evidence of a heat flux or any fluxes of elements that could have moved with the carbon dioxide.

The CO_2 rises from its sources and dissolves in the waters trapped in the near-surface soils and colluvium. This causes the formation of H_2CO_3 and thus a drop in pH, leading to the mobilization of atmospheric sourced calcium trapped in these soils. Degassing and the reaction of the K-feldspar in the rhyolite to form montmorillonite leads to a subsequent rise in pH and the precipitation of the secondary calcite.

The initiation of these alterations zones act to facilitate further reactions through a more effective trapping for both water and CO_2, prolonging the reaction times and producing a positive feedback cycle as described by Kimberley and Abu-Jaber (2005). The implications of this with regards to CCS may be significant. While it is generally assumed that CO_2 leaking out of CCS sites are best controlled by ensuring interaction with alkali-earth bearing country rock, this is not always a feasible option. In conditions where that is the case, it might be advisable to minimize re-release of CO_2 by ensuring the presence of sufficient labile calcium or magnesium bearing minerals in a clayey matrix in the near surface. Because remobilization of calcite is a carbon-neutral process, it would be advisable to choose seeding of soil covers with crushed basalt or other alkali-earth bearing silicates. By initiating the positive feedback process that seems to be operating at Wadi Namaleh, a significant portion of the carbon dioxide may permanently trapped in carbonate minerals. Initially, this process would probably not be very effective, and will only become so after the amounts of clay increase and the surface layer becomes less permeable. While this process would not do much to control massive leaks, it may be important in cases where small scale diffusion is occurring.

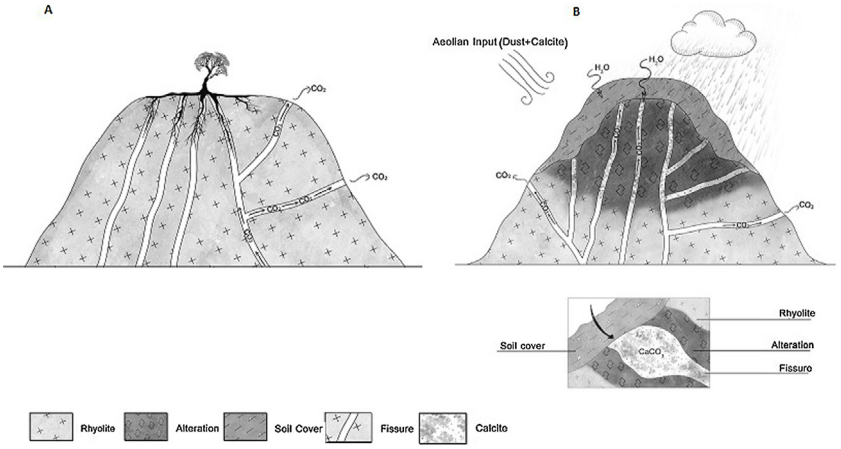

Fig. 19. A generalized schematic of how the system appears to be working. Frame A shows the case where no colluvium or soil is present, whereas frame B shows what might happen in cases where the soil cover or colluvium is present.

Acknowledgments

Thanks are due to my field assistant, Mr. Essam Abu-Jaber. I would also like to thank Dr. Mamoun Makahleh and Mrs. Sukaina Jarrar at the Jordan Atomic Energy Commission for the chemical analyses, Ms. Hadeel Hirzallah at Yarmouk University for the SEM analysis, Professor Hans Mommsen at Bonn University (Germany) for conducting the Neutron Activation Analyses, Prof. Dr. M. Joachimski and Dr. Bernhard Lucke at the Friedrich-Alexander Universitat at Erlangen, Germany for their help in analyzing the carbon and oxygen isotopes in the carbonate, Eng. Susan Kilani at the Water Authority of Jordan for analyzing the water sample for isotopic composition and Professor Chris Holmden at the University of Saskatchewan for analyzing the strontium isotopes. I would also like to extend appreciation to Tareq Bashiti for his help in preparing the thin sections. Thanks are also due to Catreena Hamarneh, Ola Rayyan, Nour Khreis and Ghusoun Zuaiter for their help with the graphics. This paper greatly benefited from the detailed and thoughtful comments of Axel Liebscher and an anonymous reviewer. This project was funded by the Abdelhamid Shoman Fund for Scientific Research (5/2015).

References

Abu-Jaber, N., El-Naser, H., 2016. Geology and hydrochemistry of the deep sandstone aquifers of Jordan. Environ. Earth Sci. 75, 875.
Abu-Jaber, N.S., Kimberley, M.M., 1992a. Origin of ultramafic-hosted vein magnesite deposits. Ore Geol. Rev. 7 (3), 155–191.
Abu-Jaber, N.S., Kimberley, M.M., 1992b. Origin of ultramafic-hosted magnesite on Margarita Island, Venezuela. Mineralium Deposita 27 (3), 234–241.
Atallah, M., Al-Bataina, B., Mustafa, H., 2001. Radon emanation along the Dead Sea transform (rift) in Jordan. Environ. Geol. 40, 1440–1446.
Avrahamov, N., Gelman, F., Yechieli, Y., Aizenshtat, Z., Nissenbaum, A., Sivan, O., 2015. Proposed sources of methane along the Dead Sea Transform. Chem. Geol. 395, 165–175.
Bajjali, W., Abu-Jaber, N., 2001. Climatological signals of the paleogroundwater in Jordan. J. Hydrol. 243 (1), 133–147.
Barjous, M., 2003. The geology of Petra and Wadi Al Lahyana area, Map Sheets No. 3050-I and 3050-IV. Natural Resources Authority of Jordan Bulletin 56, Amman.
Barjous, M., Mikbel, S., 1990. Tectonic evolution of the Gulf of Aqaba-Dead Sea transform fault system. Tectonophysics 180 (1), 49–59.
Benson, S., Cole, D., 2008. CO_2 sequestration in deep sedimentary formations. Elements 4, 325–331.
Boschi, C., Dini, A., Dallai, L., Ruggieri, G., Gianelli, G., 2009. Enhanced CO_2-mineral sequestration by cyclic hydraulic fracturing and Si-rich fluid infiltration into serpentinites at Malentrata (Tuscany, Italy). Chem. Geol. 265 (1), 209–226.
Brookins, D.G., 1989. Aqueous geochemistry of rare earth elements. Rev. Minerol. Geochem. 21 (1), 201–225.
Castorina, F., Masi, U., 2015. Sr and Nd isotopes as tracers in pedogenic studies: evidence for Saharan dust contribution to the soils of Muravera (Sardinia, Italy). Chemie der Erde-Geochemistry 75 (3), 301–315.
Cerling, T.E., 1984. The stable isotopic composition of modern soil carbonate and its relationship to climate. Earth Planet. Sci. Lett. 71 (2), 229–240.
Deuser, W.G., Degens, E.T., 1967. Carbon isotope fractionation in the system CO_2 (gas)-CO_2 (aqueous)-HCO_3-(aqueous). Nature 215, 1033–1035.
El-Naser, H., 1991. Groundwater Resources of the Deep Aquifer Systems in NW-Jordan: Hydrogeological and Hydrochemical Quasi 3-dimensional Modelling:[mit] 27 Tabellen. (Doctoral dissertation, Lehr-und Forschungsbereich Angewandte Geologie und Hydrogeologie der Universität).
Eraifej, N., 2006. Gas geochemistry and isotopic signatures in the deep thermal waters in Jordan. Frieberg Online Geology, Vol. 16. Inst. für Geologie.
Fischer, S., Liebscher, A., Wandrey, M., CO2SINK Group, 2010. CO_2–brine–rock interaction—first results of long-term exposure experiments at in situ P–T conditions of the Ketzin CO_2 reservoir. Chemie der Erde-Geochemistry 70, 155–164.
Ganor, E., Foner, H.A., 2001. Mineral dust concentrations, deposition fluxes and deposition velocities in dust episodes over Israel. J. Geophys. Res.: Atmos. (1984-2012) 106 (D16), 18431–18437.
Ganor, E., Mamane, Y., 1967. Transport of Saharan dust across the eastern Mediterranean. Atmos. Environ. 16, 581–587.
Garrels, R.M., 1984. Montmorillonite/illite stability diagrams. Clays Clay Miner. 32 (3), 161–166.
Häring, M.O., Schanz, U., Ladner, F., Dyer, B.C., 2008. Characterisation of the Basel 1 enhanced geothermal system. Geothermics 37 (5), 469–495.
Herut, B., Starinsky, A., Katz, A., 1993. Strontium in rainwater from Israel: sources, isotopes and chemistry. Earth Planet. Sci. Lett. 120 (1), 77–84.
Holzheid, A., 2016. Dissolution kinetics of selected natural minerals relevant to potential CO 2-injection sites– Part 1: A review. Chemie der Erde-Geochemistry 76 (4), 621–641.
Ibrahim, K.M., McCourt, W.J., 1995. Neoproterozoic granitic magmatism and tectonic evolution of the northern Arabian Shield: evidence from Southwest Jordan. J. Afr. Earth Sci. 20 (2), 103–118.
Inguaggiato, C., Censi, P., D'Alessandro, W., Zuddas, P., 2016. Geochemical characterisation of gases along the Dead Sea rift: evidences of mantle CO_2 degassing. J. Volcanol. Geothermal Res. 320, 50–57.
Jordan Meteorological Department, 2015. http://www.jmd.gov.jo/RainSeason.aspx (retrieved August 17, 2015).
Keating, E.H., Fessenden, J., Kanjorski, N., Koning, D.J., Pawar, R., 2010. The impact of CO_2 on shallow groundwater chemistry: observations at a natural analog site and implications for carbon sequestration. Environ. Earth Sci. 60 (3), 521–536.
Kaudse, T., 2014. Noble gases in groundwater of the Azraq Oasis, Jordan, and along the central Dead Sea Transform-Two case studies. Ph.D. Dissertation, University of Heidelberg, Germany.
Kim, S.T., O'Neil, J.R., 1997. Equilibrium and nonequilibrium oxygen isotope effects in synthetic carbonates. Geochim. Cosmochim. Acta 61 (16), 3461–3475.
Kimberley, M., Abu-Jaber, N., 2005. Shallow perched groundwater, a flux of deep CO_2, and near-surface water-rock interaction in northeastern Jordan: An example of positive feedback and Darwin's "Warm Little Pond". Precambrian Res. 137, 273–280.
Le Maitre, R.W., 1984. A proposal by the IUGS Subcommission on the Systematics of Igneous Rocks for a chemical classification of volcanic rocks based on the total alkali silica (TAS) diagram: (on behalf of the IUGS Subcommission on the Systematics of Igneous Rocks). Aust. J. Earth Sci. 31 (2), 243–255.
Little, M., Jackson, R., 2010. Potential impacts of leakage from deep CO_2 geosequestration on overlying freshwater aquifers. Environ. Sci. Technol. 44, 9225–9232.
Lo Ré, C., Kaszuba, J.P., Moore, J.N., McPherson, B.J., 2014. Fluid–rock interactions in CO_2-saturated, granite-hosted geothermal systems: implications for natural and engineered systems from geochemical experiments and models. Geochim. Cosmochim. Acta 141, 160–178.
Mommsen, H., Bentz, M., Boix, A., 2016. Provenance of red-figure pottery of the classical period excavated at olympia. Archaeometry 58, 371–379.

Powell, J.H., Abed, A., Jarrar, G.H., 2015. Ediacaran Araba complex of Jordan. GeoArabia 20, 99–156.
Pronost, J., Beaudoin, G., Tremblay, J., Larachi, F., Duchesne, J., Hébert, R., Constantin, M., 2011. Carbon sequestration kinetic and storage capacity of ultramafic mining waste. Environ. Sci. Technol. 45 (21), 9413–9420.
Quade, J., Cerling, T.E., Bowman, J.R., 1989. Systematic variations in the carbon and oxygen isotopic composition of pedogenic carbonate along elevation transects in the southern Great Basin, United States. Geolog. Soc. Am. Bull. 101 (4), 464–475.
Rempel, K.U., Liebscher, A., Heinrich, W., Schettler, G., 2011. An experimental investigation of trace element dissolution in carbon dioxide: applications to the geological storage of CO2. Chem. Geol. 289 (3), 224–234.
Rullkötter, J., Spiro, B., Nissenbaum, A., 1985. Biological marker characteristics of oils and asphalts from carbonate source rocks in a rapidly subsiding Graben, Dead Sea, Israel. Geochim. Cosmochim. Acta 49 (6), 1357–1370.
Romanek, C.S., Grossman, E.L., Morse, J.W., 1992. Carbon isotopic fractionation in synthetic aragonite and calcite: effects of temperature and precipitation rate. Geochim. Cosmochim. Acta 56 (1), 419–430.
Rutqvist, J., 2012. The geomechanics of CO_2 storage in deep sedimentary formations. Geotech. Geol. Eng. 30, 525–551.
Scheuvens, D., Schütz, L., Kandler, K., Ebert, M., Weinbruch, S., 2013. Bulk composition of northern African dust and its source sediments—a compilation. Earth-Science Rev. 116, 170–194.
Sokol, E., Kozmenko, O., Smirnov, S., Sokol, I., Novikova, S., Tomilenko, A., Kokh, S., Ryazanova, T., Reutsky, V., Bul'bak, T., Vapnik, Y., Deyak, M., 2014. Geochemical assessment of hydrocarbon migration phenomena: case studies from the south-western margin of the Dead Sea Basin. J. Asian Earth Sci. 93, 211–228.
Taylor, S.R., McLennan, S.M., 1985. The Continental Crust: Its Composition and Evolution. Blackwell Scientific Publications, pp. 1–328.
Ueda, A., Kato, K., Ohsumi, T., Yajima, T., Ito, H., Kaieda, H., Metcalf, R., Takase, H., 2005. Experimental studies of CO_2-rock interaction at elevated temperatures under hydrothermal conditions. Geochem. J. 39 (5), 417–425.
Van der Hoven, S.J., Quade, J., 2002. Tracing spatial and temporal variations in the sources of calcium in pedogenic carbonates in a semiarid environment. Geoderma 108 (3), 259–276.
Weldeab, S., Emeis, K.C., Hemleben, C., Siebel, W., 2002. Provenance of lithogenic surface sediments and pathways of riverine suspended matter in the Eastern Mediterranean Sea: evidence from $^{143}Nd/^{144}Nd$ and $^{87}Sr/^{86}Sr$ ratios. Chem. Geol. 186 (1), 139–149.
Yair, A., Karnieli, A., Issar, A., 1991. The chemical composition of precipitation and runoff water on an arid limestone hillside, northern Negev, Israel. J. Hydrol. 129 (1), 371–388.
Zhang, J., Quay, P.D., Wilbur, D.O., 1995. Carbon isotope fractionation during gas-water exchange and dissolution of CO_2. Geochim. Cosmochim. Acta 59 (1), 107–114.